IEEE Access
Multidisciplinary ⋮ Rapid Review ⋮ Open Access Journal

Received 11 December 2024, accepted 5 January 2025, date of publication 13 January 2025, date of current version 17 January 2025.

Digital Object Identifier 10.1109/ACCESS.2025.3529307

RESEARCH ARTICLE

A Pedaling Torque Observation Approach for Sensorless Electric Bicycles

RICCARDO MANDRIOTA, NIKLAS KÖNIG, EMANUELE GRASSO, AND MATTHIAS NIENHAUS

Lehrstuhl für Antriebstechnik, Universität des Saarlandes, 66123 Saarbrücken, Germany

Corresponding author: Riccardo Mandriota (mandriota@lat.uni-saarland.de)

ABSTRACT This study proposes an innovative unknown input observation approach based on Kalman filtering to estimate the cycling torque and provide assistance in electrically powered bicycles. Specifically, a constant and a sinusoidal pedaling torque model are compared, underlining the need for an enhanced mathematical description to improve system performance. Using a nonlinear model of the bicycle longitudinal dynamics, the cycling torque is reconstructed with an Extended Kalman Filter. Also, an online low-computational effort road slope estimation method based on Kalman filtering, that accounts for cornering effect errors, is proposed. The considered approaches, that utilize wheel speed, inertial, and motor current measurements, are tested in an outdoor setting with variable slopes and curves. Differently from the current state-of-the-art, the estimation performances are not only expressed in terms of pedaling torque estimation error minimization. This work presents a novel pedaling power and delivered energy analysis to evaluate the provided electrical assistance and the consequent pedaling effort decrease. The experimental results show that a cycling endeavor reduction, similar to what can be achieved when electrical assistance is provided employing a torque sensor, is possible, especially when relying on improved pedaling modeling.

INDEX TERMS Electric bicycles, Kalman filtering, pedaling torque estimation, road slope estimation, sensorless control, state observation.

I. INTRODUCTION

In the early 2000s, the popularization of lithium batteries made weight reduction and increased electrical autonomy in light electric vehicles possible. Such innovations generated a still ongoing worldwide boom in the market of these vehicles, and in particular in the electric bicycle one [1]. Nowadays, government policies promote light electric vehicles as a possible means of transportation to reduce atmospheric pollution, counteract global warming, and decrease traffic congestion in our cities [2]. Among these vehicles, electric bicycles may encourage physical activity and rehabilitate people with health problems [3]. Indeed, compared to standard bicycles, the motor electrical assistance reduces cycling efforts even in the presence of variable ground reliefs without losing the training aspect as in electric scooters. Nevertheless, high costs make electric bicycles not affordable to a part of the population. The price of an electric bicycle is related to its design characteristics because there are different ways to provide electrical assistance depending on the type of motor, controller, and sensors employed. Sensing elements, such as pedaling torque and cadence sensors, are needed to provide electrical assistance following the local legislation that limits the maximum deliverable power at defined speed levels, the maximum vehicle weight, and the kind of assistance. Additionally, their installation requires a proper design of the bicycle frame. Also, they are mounted on bicycle parts where the pedaling force, shock, and vibrations are directly applied determining a cost increase. High-quality sensors can amount to around $10 - 15\%$ of the overall cost of the vehicle. Therefore, to simplify the mechanical design and decrease the final price of the vehicle, sensorless control approaches for electric bicycles have been investigated in the last decade.

Torque-sensorless control for electric bicycles refers mainly to control strategies that provide electrical aid without

The associate editor coordinating the review of this manuscript and approving it for publication was Wei Xu.

utilizing pedaling torque sensors. Other low-cost sensors such as current, rotor position, speed, or Inertial Measurement Units (IMUs) are still employed to estimate the cycling torque and provide motor assistance accordingly. Pedaling torque estimation approaches are based on the assumption of considering the human action as an unknown input or disturbance acting on the vehicle dynamics. The first approaches to estimate disturbances applied to a system were based on a state-space representation and called Unknown Input Observers (UIOs) [4]. Later, this problem was reformulated in the Laplace domain using the so-called Disturbance OBservers (DOBs) [5]. As proposed in [6], a Reaction Force Observer (RFO), which employs a more complex structure constituted of a cascade of two DOBs, allows for improved torque estimation compared to the classical DOB. Nevertheless, all the approaches mentioned before have a model-based structure that deteriorates the estimation accuracy in the presence of modeling errors and parametric variations [7].

In the last decade, disturbance estimation approaches have been applied to the field of electric bicycles. Some methods describe the pedaling torque utilizing a constant model, namely considering the bandwidth of the disturbance smaller than the observer dynamics. A DOB approach estimates the pedaling torque in [8]. However, the validity of the method is limited to the case of the absence of environmental forces in the vehicle dynamic model such as gravity and friction. Another DOB-based method, which estimates and compensates for the environmental forces, is proposed in [9]. In this work, the human torque is determined by analyzing the dynamics of the crankset mechanism exploiting IMU measurements. A RFO-based approach has been also investigated in [10]. This method consists of an inner DOB that estimates and rejects external disturbances and an additional DOB employed to extract the pedaling torque and tuned with a lower bandwidth selected according to considerations on the maximum pedaling torque frequency. To reject low-frequency environmental disturbances and extract the pedaling torque, the previously described method is enhanced by employing a band-pass filter in the works [11] and [12]. The cycling torque estimation problem has been also addressed employing an UIO in [13], where a Kalman Filter (KF) is utilized as a state observer. However, the validity of the approach has been tested only under laboratory conditions. Likewise, [14] proposes an UIO-based method that employs an Unscented Kalman Filter (UKF). This approach presents a contemporary estimation of the road slope using an adaptive orthogonal filter based on IMU measurements to improve the torque estimation.

In the works based on a constant pedaling torque model, the experimental results show that they allow only an approximate estimate of the average applied cycling. As stated in [15], a detailed disturbance modeling may improve the estimation accuracy. Hence, some studies consider the pseudo-periodicity of cycling in the employed model. A Fourier analysis of the total disturbance estimated by a DOB is used in [16] to extract the pedaling torque information. The same approach is then enhanced in [17] to estimate and compensate external disturbances utilizing a Recursive Least Squares (RLS) algorithm and in [18] to improve the estimation during the first pedaling cycle when no previous information on the cycling torque is available. Also, [19] proposes an UIO-based approach that models the disturbance as the sum of a sine with variable frequency plus a bias. In particular, this work exploits a state augmentation of a Luenberger observer and a simultaneous estimation of the pedaling frequency obtained by an adaptive notch filter.

Although many torque-sensorless control techniques for electric bicycles can be already found in the literature, there are still extensive improvement margins. Among the possible employable methods previously discussed, this work focuses on the utilization of UIOs, i.e. state observation approaches. Firstly in the literature, the so-called Pedaling Torque Observers (PTOs), based on the utilization of pedaling torque models of different complexity, namely a constant and a periodic model, are discussed and compared extensively. Differently from other works on this topic, the electrical assistance performances are expressed not only in terms of pedaling torque estimation error minimization. Indeed, an analysis of the delivered pedaling power and energy under defined riding conditions is proposed as a metric to evaluate the cycling effort reduction capability of torque-sensorless control approaches. Among the possible state observers employable to address the torque estimation problem, the Extended Kalman Filter (EKF) is selected here because of its capability of easily handling non-severe nonlinear systems, such as the one under investigation, and its comprehensible tuning based on weighing the confidence on model and measurements through filter covariance matrices. Furthermore, to compensate for the effect of gravity in the torque estimator, a low-complexity online road slope estimation in the form of a KF based on a low-cost IMU and vehicle speed measurement is proposed in this work.

Following, the structure of this work is briefly reported. In Section II, the generic mathematical model of the bicycle longitudinal dynamics and an analysis of the pedaling torque profiles are presented. Afterwards, the simplifying assumptions made to integrate these models into a PTO structure are reported. In Section III, the PTOs are expressed mathematically in the form of EKFs. Then, the impact of inputs and measurements of the PTOs on the pedaling torque estimation and the proposed road slope estimation algorithm are discussed in Section IV. Section V contains the experimental validation of the torque-sensorless control algorithms. Section VI concludes this work and prospects future improvements to the proposed techniques.

II. MATHEMATICAL MODELING

When designing electric bicycles, a mathematical model is used to evaluate the combined human-motor power needed

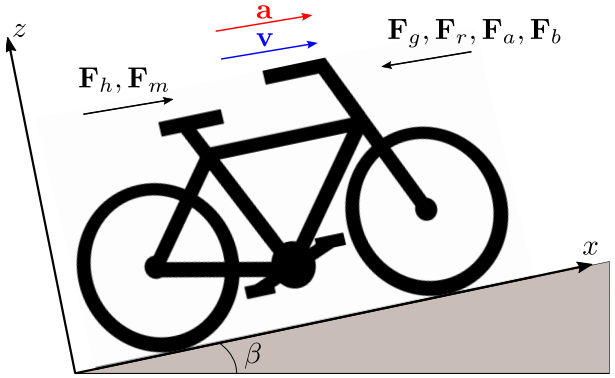

FIGURE 1. Bicycle longitudinal dynamics including the effects of driving and resisting forces.

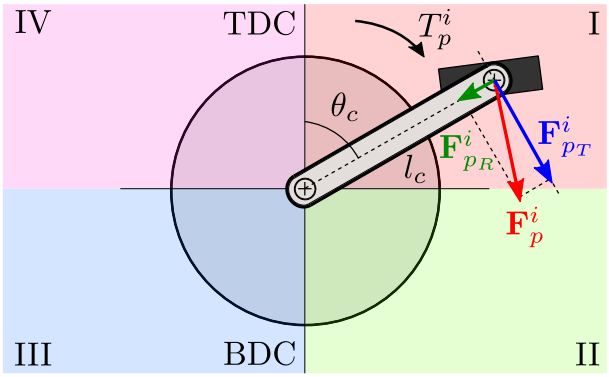

FIGURE 2. Single pedaling torque contribution T_p^i to the global pedaling torque T_p over one crank angle θ_c revolution, with $i \in \{l, r\}$.

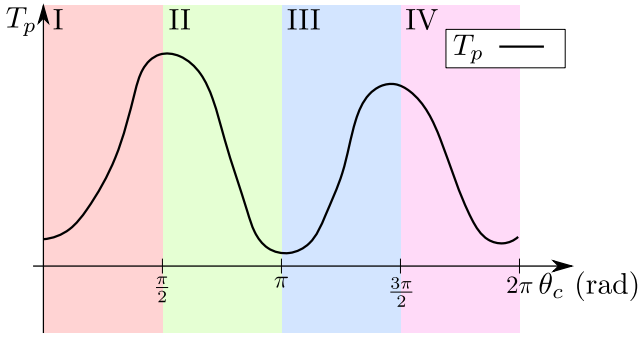

FIGURE 3. Typical pedaling torque profile T_p over one crank angle θ_c revolution.

for hill-climbing and overcoming the wind and rolling resistances [20]. The vehicle dynamics analysis can be reduced to the longitudinal direction of motion x because the rider stabilizes the vehicle through the steering action of the handlebar [21]. Under these hypotheses, the bicycle dynamics, illustrated in Fig. 1, can be expressed as follows:

$$\underbrace{\eta_d \frac{T_p}{r\tau_d} + F_h^e}_{F_h} + \underbrace{\eta_m \frac{T_m}{r\tau_m}}_{F_m} - \underbrace{mg\sin(\beta)}_{F_g} - \underbrace{\mu mg\cos(\beta)}_{F_r} - \underbrace{\operatorname{sgn}(v_a)\frac{1}{2}\rho A_d v_a^2}_{F_a} - F_b = ma, \tag{1}$$

where T_p is the pedaling torque, η_d and τ_d are the drivetrain efficiency and its gear ratio, r is the wheel radius, F_h^e are the other human forces not applied at the pedals, T_m is the motor torque, η_m and τ_m are the motor transmission efficiency and its gear ratio, m is the system mass, g is the gravity acceleration on Earth, β is the road grade, μ is the rolling friction coefficient, $v_a = v + v_w$ is the relative air speed along the longitudinal direction equal to the sum of the longitudinal vehicle speed v and the longitudinal wind speed v_w, ρ is the air density, A_d is the drag area, and a is the longitudinal vehicle acceleration. Also, F_h, F_m, F_g, F_r, F_a, F_b represent the human, motor, gravity, rolling friction, aerodynamic drag, and braking force contributions, respectively.

A. HUMAN FORCES

The pedaling torque estimation requires an analysis of the human input forces applied to the bicycle and the pedaling torque profile to improve the disturbance modeling. The pedaling torque T_p has a time-variant profile related to the crankset mechanism geometry, the intensity, and the direction of the forces applied to the pedals. This torque is equal to the sum of the contributions of the left T_p^l and right T_p^r pedals:

$$T_p = T_p^l + T_p^r. \tag{2}$$

Each one of them is generated by the tangential components to the pedal motion of the left F_{pT}^l and right F_{pT}^r pedaling forces, whereas the radial components F_{pR}^l and F_{pR}^r are not contributing to the torque generation and thus referred to as ineffective components. Based on these considerations, (2) can be written as:

$$T_p = \left(F_{pT}^l + F_{pT}^r\right) l_c, \tag{3}$$

where l_c is the length of the crank arm. Fig. 2 represents the single pedal torque contribution to the total pedaling torque over one crank angle θ_c revolution. Considering $\theta_c = 0$ rad when one pedal is at the Top Dead Center (TDC), a propulsive torque contribution T_p^i, where $i \in \{l, r\}$, is generated in the first half period (I and II quarters). During the second half period (III and IV quarters), the single torque contribution can have a negative value because non-professional cyclists do not lift the leg while pushing the pedal with the other one [22]. Since each pedal alternates a propulsive and a recovery phase, the total generated torque results in a quasi-periodic pedaling torque profile similar to a sinusoidal signal with an offset [16], [19]. In particular, the total pedaling torque T_p typically presents two maximums when the pedals are close to the horizontal position ($\theta_c \simeq \frac{\pi}{2}$ rad and $\theta_c \simeq \frac{3\pi}{2}$ rad) and two minimums close to the TDC and the Bottom Dead Center (BDC) ($\theta_c \simeq 0$ rad and $\theta_c \simeq \pi$ rad). Therefore, the pedaling torque presents a second harmonic of the crank angle. Fig. 3 illustrates a typical pedaling torque profile.

From these considerations, a simplified mathematical expression of the pedaling torque can be derived:

$$T_p(t) = T_{p_0} - T_{p_2}\cos\left[2\theta_c(t) + \theta_c(0)\right], \tag{4}$$

where T_{p_0} is the continuous component or pedaling torque offset, T_{p_2} is the amplitude of the pedaling torque second harmonic, and $\theta_c(0)$ is the crank angle initial value that depends on the initial position of the pedals when starting pedaling. It has to be remarked that (4) represents a generic mathematical expression that will be used to improve the disturbance modeling and, thus, the pedaling torque estimation. Cycling profiles may contain complex-to-model high-order harmonics dependent on the riding conditions, the pedaling style of the cyclist, inter-subject variability, and the mechanical configuration of the bicycle. Besides pedaling, a cyclist propels a bicycle with muscles other than the legs or pushing the vehicle while walking. The term F_h^e includes all these force contributions external to the crankset.

B. SIMPLIFIED MODEL

In electric bicycles, the highest electrical assistance is typically required at low speeds during the acceleration phases or hill climbing rather than at high speeds where the motor aid may be dangerous or not admitted by the local legislation. As stated in [23], the gravity resistance has the highest impact on the vehicle dynamics in variable inclines. Moreover, in level ground riding at low speeds, the rolling resistance has a higher impact than the aerodynamic one that becomes predominant over $v \simeq 11$ km/h.

As stated in Section I, disturbance estimation approaches require a correct knowledge of the model parameters. However, many of these are time-variant and cannot be measured or estimated online without increasing the system complexity. In the following, the simplifying assumptions made on the bicycle longitudinal model in this work are reported:

- Since the gravity resistance is predominant in inclines, a correct system mass m and road slope β knowledge is fundamental. While the mass can be considered constant during cycling, the road angle may vary rapidly and require an online estimation.
- Although time-variant, parameters such as the rolling friction μ, the drag area A_d, and the air density ρ can be considered constant because their impact is smaller than the one of gravity resistance variations and an online estimation would require the employment of additional sensors or estimation techniques determining an increase in the system complexity.
- Likewise, the effect of wind is neglected in this work ($v_w = 0$ km/h) since typically negligible in the low-speed range except in the rare case of strong headwinds.
- Power losses in the mechanical transmissions are also neglected ($\eta_d = \eta_m = 1$) since the latter are typically characterized by high efficiency in bicycle applications. Also, the gear ratios τ_d and τ_m are considered constant, i.e. gear variations are neglected.
- Braking forces F_b and human propulsive forces not generated by pedaling F_h^e are not considered in the employed model.
- The model is derived under the assumption of no wheel-slipping and engaged drivetrain.

Under these hypotheses, (1) can be reduced to:

$$\frac{T_p(t)}{r\tau_d} + \frac{T_m(t)}{r\tau_m} - mg\sin(\beta(t)) - \mu mg\cos(\beta(t)) - \frac{1}{2}\rho A_d v^2(t) = m\frac{dv(t)}{dt}, \tag{5}$$

where the vehicle longitudinal acceleration is expressed as the derivative of its speed $a(t) = \frac{dv(t)}{dt}$ and the time dependency of the considered time-variant quantities is explicitly reported. Considering the effect of the rolling resistance as the one of an apparent road slope $\beta_\mu = \arctan(\mu)$ and applying trigonometric considerations, (5) can be reduced to:

$$\frac{T_p(t)}{r\tau_d} + \frac{T_m(t)}{r\tau_m} - \frac{mg}{\cos(\beta_\mu)}\sin(\beta(t) + \beta_\mu) - \frac{1}{2}\rho A_d v^2(t) = m\frac{dv(t)}{dt}. \tag{6}$$

Since within the possible realistic range of $\mu \in [0.002; 0.01]$ defined in [27], $\mu \simeq \beta_\mu$ and $\cos(\beta_\mu) \simeq 1$, (6) can be written as:

$$\frac{T_p(t)}{r\tau_d} + \frac{T_m(t)}{r\tau_m} - mg\alpha(t) - \frac{1}{2}\rho A_d v^2(t) = m\frac{dv(t)}{dt}, \tag{7}$$

where $\alpha(t) = \sin(\beta(t) + \mu)$.

III. PEDALING TORQUE OBSERVATION

In this work, the pedaling torque estimation is performed employing two PTOs expressed in the form of EKFs based on different models of the pedaling torque, a constant (CPTO) and a sinusoidal (SPTO) one. After providing the necessary background on the state observer selection and Kalman filtering, both PTOs are expressed mathematically.

A. STATE OBSERVER SELECTION

As shown in [24], a system internal state observation can be performed utilizing several kinds of state observers. The well-known Luenberger observer might be employed to address the problem of disturbance estimation. Nevertheless, even in its nonlinear and extended forms, the observer design is heavily dependent on the accuracy of the mathematical model of the plant [25]. Thus, poor performances would be achieved in the presence of uncertainty, measurement noise, and modeling simplifications like in the case under investigation. To overcome these issues, the KF is one prominent estimator that minimizes a cost function based on mathematical assumptions about the disturbances acting on the system. Under the hypotheses of a sufficiently accurate model affected by stochastic, white, and Gaussian disturbances with known covariance, the KF provides an optimal solution that minimizes the 2-norm of the estimation error, namely the mean squared estimation error [24]. Although the KF has been originally defined for linear discrete-time systems, it can be easily extended to the case of nonlinear systems employing the extended form EKF. In this

approach, the nonlinear discrete-time system is linearized around a nominal state trajectory, utilizing the KF state estimate as a nominal trajectory. The performed system linearization can introduce estimation errors depending on the severity of the nonlinearity. The UKF could be used to improve the estimation performances in nonlinear systems. However, its increased complexity makes it impractical for many applications. Another renowned approach to dealing with nonlinear uncertain systems is the Sliding Mode Observers (SMO). Although characterized by high robustness to parametric variations and easy implementation, it introduces chattering on the state estimation that makes it undesirable in practical employments [25].

Based on the considerations above, the EKF has been considered in this work due to its optimal estimation capability in the presence of noise and its comprehensible tuning based on the selection of the covariance matrices that allow the state estimation even in the presence of nonlinearities and modeling simplifications. Although the linearization represents an approximation, the introduced linearization error can be neglected in the case of non-severe nonlinearities, like in the system under investigation. Furthermore, Kalman filtering has been widely applied in many engineering fields including trajectory estimation, state and parametric estimation for control and diagnosis, data merging, signal processing, etc. [26]. Therefore, the EKF represents a commonly utilized, simple, and comprehensible solution to address nonlinear state estimation problems such as pedaling torque estimation. For the sake of brevity, the KF and EKF algorithms are not reported in this work. Detailed information about the two algorithms can be found in [28].

B. CONSTANT PEDALING TORQUE OBSERVER

In the CPTO, the pedaling torque is considered constant, namely the unknown disturbance bandwidth is assumed to be smaller than the natural response of the observer:

$$\frac{dT_p(t)}{dt} = 0. \tag{8}$$

Discretizing (7) and (8) with the sampling time T_s, a nonlinear discrete-time state-space model of the system that considers $\mathbf{x}(k) = \begin{bmatrix} v(k) & T_p(k) \end{bmatrix}^T$ as the state vector, $\mathbf{u}(k) = [T_m(k) \quad \alpha(k)]^T$ as the input vector, and $y(k) = v(k)$ as the measurement can be obtained:

$$\begin{cases} v(k) = \left[1 - \dfrac{\rho A_d T_s}{2m} v(k-1)\right] v(k-1) \\ \quad + \dfrac{T_s}{mr\tau_d} T_p(k-1) + \dfrac{T_s}{mr\tau_m} T_m(k-1) \\ \quad - gT_s\alpha(k-1) + w_v(k-1) \\ \\ T_p(k) = T_p(k-1) + w_{T_p}(k-1) \end{cases}, \tag{9}$$

$$y(k) = v(k) + v_v(k), \tag{10}$$

where $\mathbf{w}(k) = \begin{bmatrix} w_v(k) & w_{T_p}(k) \end{bmatrix}^T$ is the noise on the process and $v(k) = v_v(k)$ is the noise on the measurement. These white and Gaussian stochastic processes can be described by the covariance matrices:

$$\mathbf{Q} = \begin{bmatrix} \sigma_{w_v}^2 & 0 \\ 0 & \sigma_{w_{T_p}}^2 \end{bmatrix}, \quad R = \sigma_{v_v}^2, \tag{11}$$

where $\sigma_{w_v}^2$, $\sigma_{w_{T_p}}^2$, and $\sigma_{v_v}^2$ are the variances of the noises w_v, w_{T_p}, and v_v, respectively. Considering as initial state $\mathbf{x}(0) = [0 \quad 0]^T$ and the estimation error covariance matrix $\mathbf{P} = \mathbf{I} \in \mathbb{R}^{2\times 2}$, where $\mathbf{I}$ represents the identity matrix, the EKF algorithm can be applied to obtain the pedaling torque estimation $\hat{T}_p(k)$ at each step.

C. SINUSOIDAL PEDALING TORQUE OBSERVER

In the case of the SPTO, the CPTO structure is enhanced including the sinusoidal pedaling torque model (4) through a state augmentation:

$$\mathbf{x}(t) = \begin{bmatrix} v(t) & \xi_0(t) & \xi_2^c(t) & \xi_2^s(t) \end{bmatrix}^T, \tag{12}$$

where $\xi_0(t) = T_{p_0}$, $\xi_2^c(t) = -T_{p_2}\cos[2\theta_c(t) + \theta_c(0)]$, and $\xi_2^s(t) = T_{p_2}\sin[2\theta_c(t) + \theta_c(0)]$. Thus, (4) can be written as the sum of the states:

$$T_p(t) = \xi_0(t) + \xi_2^c(t). \tag{13}$$

The continuous component of the pedaling torque can be considered constant with respect to the observer dynamics:

$$\frac{d\xi_0(t)}{dt} = 0. \tag{14}$$

In the case of engaged drivetrain, the crankset angular speed can be expressed as a function of the bicycle speed $\omega_c(t) = \frac{v(t)}{r\tau_d}$. Thus, the derivatives of $\xi_2^c(t)$ and $\xi_2^s(t)$ can be written as:

$$\frac{d\xi_2^c(t)}{dt} = \frac{2}{r\tau_d} v(t)\,\xi_2^s(t), \tag{15}$$

$$\frac{d\xi_2^s(t)}{dt} = -\frac{2}{r\tau_d} v(t)\,\xi_2^c(t). \tag{16}$$

Discretizing (7), (14), (15), and (16) with the sampling time T_s, a nonlinear discrete-time state-space model of the system that considers the discretized version of the state vector (12) and the same input vector and measurement of the CPTO, can

be derived:

$$\begin{cases} v(k) = \left[1 - \dfrac{\rho A_d T_s}{2m} v(k-1)\right] v(k-1) \\ + \dfrac{T_s}{mr\tau_d} \xi_0(k-1) + \dfrac{T_s}{mr\tau_d} \xi_2^c(k-1) \\ + \dfrac{T_s}{mr\tau_m} T_m(k-1) - g T_s \alpha(k-1) + w_v(k-1) \\ \xi_0(k) = \xi_0(k-1) + w_{\xi_0}(k-1) \\ \xi_2^c(k) = \xi_2^c(k-1) + \dfrac{2T_s}{r\tau_d} v(k-1)\, \xi_2^s(k-1) \\ + w_{\xi_2^c}(k-1) \\ \xi_2^s(k) = \xi_2^s(k-1) - \dfrac{2T_s}{r\tau_d} v(k-1)\, \xi_2^c(k-1) \\ + w_{\xi_2^s}(k-1) \end{cases}, \tag{17}$$

$$y(k) = v(k) + v_v(k), \tag{18}$$

where the white and Gaussian noises on the process $\mathbf{w}(k) = \begin{bmatrix} w_v(k) & w_{\xi_0}(k) & w_{\xi_2^c}(k) & w_{\xi_2^s}(k) \end{bmatrix}^T$ and the measurements $v(k) = v_v(k)$ are considered. These stochastic processes can be described by the covariance matrices:

$$\mathbf{Q} = \begin{bmatrix} \sigma^2_{w_v} & 0 & 0 & 0 \\ 0 & \sigma^2_{w_{\xi_0}} & 0 & 0 \\ 0 & 0 & \sigma^2_{w_{\xi_2^c}} & 0 \\ 0 & 0 & 0 & \sigma^2_{w_{\xi_2^s}} \end{bmatrix}, \quad R = \sigma^2_{v_v}, \tag{19}$$

where $\sigma^2_{w_{\xi_0}}$, $\sigma^2_{w_{\xi_2^c}}$, and $\sigma^2_{w_{\xi_2^s}}$ are the variances of the noises w_{ξ_0}, $w_{\xi_2^c}$, and $w_{\xi_2^s}$ respectively. Considering as initial state $\mathbf{x}(0) = [0 \;\; 0 \;\; 0 \;\; 0]^T$ and the error covariance matrix $\mathbf{P} = \mathbf{I} \in \mathbb{R}^{4\times4}$, the EKF algorithm can be applied and the pedaling torque can be estimated at each step as follows:

$$\hat{T}_p(k) = \hat{\xi}_0(k) + \hat{\xi}_2^c(k), \tag{20}$$

where $\hat{\xi}_0(k)$, $\hat{\xi}_2^c(k)$ are the estimated states ξ_0, and ξ_2^c, respectively.

IV. PEDALING TORQUE OBSERVERS INPUTS AND MEASUREMENTS

Besides a correct knowledge of the bicycle longitudinal dynamics parameters, an accurate pedaling torque estimation requires the correctness of the inputs $\mathbf{u}(k)$ and the measurement $y(k)$ employed in the EKFs, namely the motor torque T_m, the road slope β, and the bicycle speed v. This section analyzes them and proposes a KF filter to estimate the road slope. Also, a method to compensate for modeling simplifications while cornering is discussed.

A. MOTOR TORQUE

The accuracy in the knowledge of the motor torque is dependent on the motor electrical parameters, the current measurements, and the rotor position. In the typical case of Permanent Magnet Synchronous Machines (PMSMs) with superficially mounted magnets ($L_d \simeq L_q$) employed to electrically aid the bicycle motion, the delivered torque is expressed as:

$$T_m = \frac{3}{2} n_p \Psi_{PM} i_q = k_T i_q, \tag{21}$$

where L_d is the inductance of the d-axis, L_q is the inductance of the q-axis, n_p is the number of polepairs, Ψ_{PM} is the permanent magnets flux linkage, $k_T = \frac{3}{2} n_p \Psi_{PM}$ is the motor torque constant, and i_q is the motor current along the q-axis of the rotor reference frame. Therefore, errors in the knowledge of the flux linkage or electrical parameters may introduce errors in the torque and degrade the motor control performances. Furthermore, noisy current measurements would propagate on the motor torque introducing errors in the motor control. Likewise, errors in the rotor position affect the coordinate transformation and propagate on the measured torque.

B. ROAD SLOPE

As previously stated, road angle variations affect considerably the vehicle dynamics and can introduce significant errors in the pedaling torque estimation. Among the possible approaches that achieve an online road grade estimation, this work proposes a method based on the vehicle longitudinal kinematics and a reduced set of inertial measurements provided by a low-cost Micro-ElectroMechanical System (MEMS) IMU. As shown in [29], such methods allow to reduce the computational complexity and achieve a comparable accuracy to approaches based on a vehicle three-dimensional kinematic modeling and that use a complete set of inertial measurements like in the works [29], [30].

After calibrating and compensating for the mounting offsets, the IMU acceleration measurements $\mathbf{a}_m$ during vehicle accelerations $a \neq 0\ \mathrm{m/s^2}$ can be expressed as:

$$\mathbf{a}_m = \mathbf{g} + \mathbf{a}, \tag{22}$$

namely, the device measures the overall acceleration equal to the sum of gravity and vehicle acceleration. Fig. 4 contains an example of the IMU acceleration measurements in the presence of a road slope and longitudinal acceleration when the vehicle leaning is negligible. It has to be remarked that MEMS accelerometers read gravitational field components aligned with a sensing axis of the device with a negative sign, whereas acceleration components are read with a positive sign.

This work proposes a state observer that models the bicycle longitudinal acceleration a and the gravity acceleration longitudinal component g_x as constants exploiting an UIO approach, namely considering their bandwidth smaller than the one of the observer, to estimate the road slope β. In particular, a linear discrete-time state-space model in the form of a KF that assumes as state $\mathbf{x}(k) = [a(k) \quad v(k) \quad g_x(k)]^T$

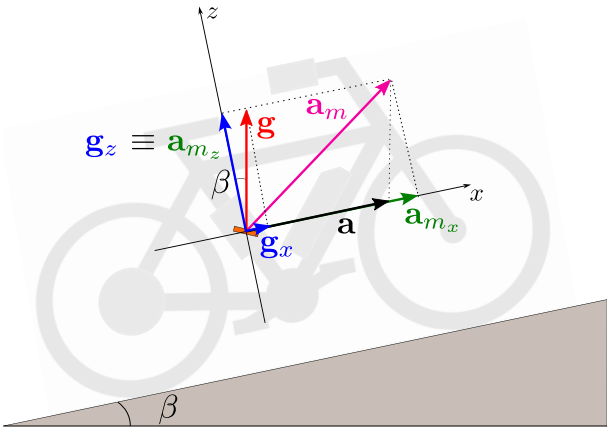

FIGURE 4. IMU measured acceleration components $\mathbf{a_m}$, after mounting offsets compensation, in the presence of a road slope, longitudinal acceleration, and no leaning.

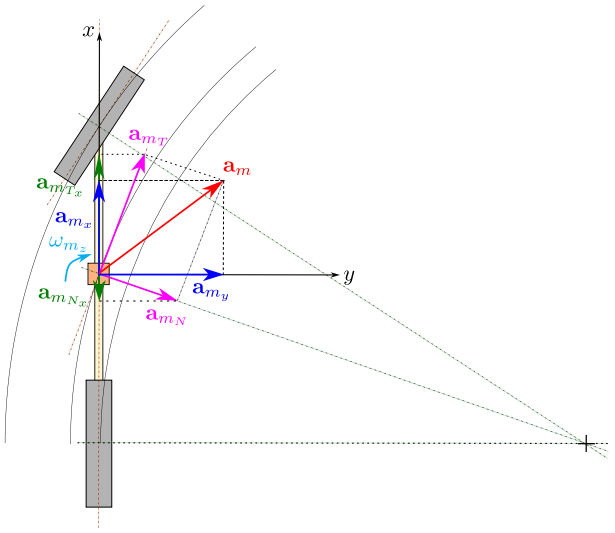

FIGURE 5. Effect of cornering on the measured IMU acceleration a_m.

and as measurements $\mathbf{y}(k) = \begin{bmatrix} v(k) & a_{m_x}(k) \end{bmatrix}^T$ is derived:

$$\begin{bmatrix} a(k) \\ v(k) \\ g_x(k) \end{bmatrix} = \begin{bmatrix} 1 & 0 & 0 \\ T_s & 1 & 0 \\ 0 & 0 & 1 \end{bmatrix} \begin{bmatrix} a(k-1) \\ v(k-1) \\ g_x(k-1) \end{bmatrix} + \begin{bmatrix} w_a(k-1) \\ w_v(k-1) \\ w_{g_x}(k-1) \end{bmatrix}, \tag{23}$$

$$\begin{bmatrix} y_1(k) \\ y_2(k) \end{bmatrix} = \begin{bmatrix} 0 & 1 & 0 \\ 1 & 0 & 1 \end{bmatrix} \begin{bmatrix} a(k) \\ v(k) \\ g_x(k) \end{bmatrix} + \begin{bmatrix} \nu_v(k) \\ \nu_{a_{m_x}}(k) \end{bmatrix}, \tag{24}$$

where white and Gaussian noises on the process $\mathbf{w}(k) = \begin{bmatrix} w_a(k) & w_v(k) & w_{g_x}(k) \end{bmatrix}^T$ and on the measurements $\nu(k) = \begin{bmatrix} \nu_v(k) & \nu_{a_{m_x}}(k) \end{bmatrix}^T$ are considered. These stochastic processes can be described by the covariance matrices:

$$\mathbf{Q} = \begin{bmatrix} \sigma^2_{w_a} & 0 & 0 \\ 0 & \sigma^2_{w_v} & 0 \\ 0 & 0 & \sigma^2_{w_{g_x}} \end{bmatrix}, \quad \mathbf{R} = \begin{bmatrix} \sigma^2_{\nu_v} & 0 \\ 0 & \sigma^2_{\nu_{a_{m_x}}} \end{bmatrix}, \tag{25}$$

where $\sigma^2_{w_a}$, $\sigma^2_{w_v}$, $\sigma^2_{w_{g_x}}$, $\sigma^2_{\nu_v}$, and $\sigma^2_{\nu_{a_{m_x}}}$ are the variances of the noises w_a, w_v, w_{g_x}, ν_v, and $\nu_{a_{m_x}}$, respectively. Considering as initial state $\mathbf{x}(0) = [0 \quad 0 \quad 0]^T$ and as error covariance matrix $\mathbf{P} = \mathbf{I} \in \mathbb{R}^{3\times3}$, the estimated $\hat{g}_x(k)$ can be employed to obtain the road grade at each step of the algorithm using the expression:

$$\hat{\beta}(k) = \arcsin\left(\frac{\hat{g}_x(k)}{g}\right). \tag{26}$$

where $\hat{\beta}(k)$ is the estimated road slope.

Estimation methods based only on the longitudinal motion of the vehicle are nonetheless limited by modeling simplifications. The employed model neglects the effect of cornering while riding that introduces centrifugal acceleration components, measured by the IMU, that can degrade the accuracy of the road angle estimation. Fig. 5 illustrates a two-dimensional model of a bicycle containing the measured acceleration components when riding in a curve. Considering the IMU mounted in a generic position of the bicycle frame, the measured longitudinal acceleration a_{m_x} always corresponds to the direction of the frame that can differ from the one tangential to the instantaneous trajectory. Thus, the centrifugal acceleration a_{m_N}, whose direction is normal to the instantaneous trajectory, may not be normal to the longitudinal direction of the IMU determining a measurement offset $a_{m_{N_x}}$ that propagates onto the acceleration measurement $a_{m_x} = a_{m_{T_x}} - a_{m_{N_x}}$. Under these conditions, the measured longitudinal acceleration differs from the instantaneous tangential acceleration $a_{m_x} \neq a_{m_T}$, determining errors in the road grade estimation. To overcome this issue, the IMU might be mounted into the wheels where the longitudinal direction of the sensor corresponds to the one tangential to the instantaneous trajectory. However, this is not a good practical approach because the measured accelerations would be more affected by vibrations due to direct contact with the irregular road surface. Therefore, a stronger low-pass filtering that degrades the road angle estimation performance would be required. To mitigate the cornering errors, this work employs a method, proposed in [29], that filters the road angle estimate depending on the measured angular speed along the z-axis ω_{m_z} given by the IMU gyroscope, whose magnitude represents the aggressiveness of the curve. When riding in aggressive curves, the estimated slope $\hat{\beta}$ is filtered with a lower bandwidth. The curve aggressiveness is quantified through the index:

$$\Lambda = G_{\omega_{m_z}}(s)\,|\omega_{m_z}|, \tag{27}$$

where $G_{\omega_{m_z}}(s)$ is a low-pass filter expressed in the Laplace s-domain, and the magnitude of the measured IMU angular speed treats left and right-hand curves identically. The agressiveness index (27) is used to calculate the cutoff frequency f_{c_β} of a further first order low-pass filter $G_\beta(s)$ that

filters the road angle estimation:

$$f_{c_\beta} = \frac{f_{c_\beta}^{max}}{c\,(\Lambda - \Lambda_{th})} \quad \text{with} \quad f_{c_\beta} \in \left[f_{c_\beta}^{min}; f_{c_\beta}^{max}\right], \tag{28}$$

where Λ_{th} is a threshold employed to activate the filter bandwidth variation, and c is a coefficient used to adjust the celerity of this variation.

C. BICYCLE SPEED

The vehicle longitudinal speed, considered as measurement in both PTOs, is also indirectly obtained from the wheel angular speed ω. In particular, it can be calculated as follows:

$$v = \omega r = \frac{\omega_e r}{n_p}, \tag{29}$$

where the electrical angular speed $\omega_e = \frac{d\theta_e}{dt}$ is obtained by evaluating the derivative of the measured electrical rotor position θ_e. However, differentiating the measured position results in high-frequency noise amplification. Therefore, a low pass filtering of the speed is necessary and may introduce delays that propagate onto the estimation algorithms, affecting their accuracy and the responsiveness of the motor control. This means a trade-off filter bandwidth must be selected depending on the characteristics of the employed rotor position sensor and the desired control performance.

V. EXPERIMENTAL RESULTS

This section contains the experimental validation of the proposed sensorless control techniques. Firstly, an overview of the suggested control approach is provided. Then, the characteristics of the prototype utilized to perform the experiments are described. Afterwards, guidelines on the tuning of the estimation algorithms are reported. Later, the conditions under which the validation has been executed are detailed. An analysis of the torque estimation error, the pedaling power, and the delivered energy is then reported.

A. SYSTEM DESCRIPTION

In this work, the proposed torque-sensorless bicycle control, illustrated in Fig. 6, is implemented by substituting the torque sensor with current sensors, a rotor position sensor, and a six-axes IMU. The measured phase currents $\mathbf{i}_{abc} = [i_a \quad i_b \quad i_c]^T$ and the electrical rotor position θ_e are utilized to control the torque T_m of a PMSM to a target value T_m^* relying on a Field Oriented Control (FOC). The bicycle longitudinal speed v is obtained by differentiating the position sensor measurement using (29). The measured speed and the longitudinal acceleration measurement provided by the IMU a_{m_x} are the inputs of the road slope observer proposed in Section IV-B. To compensate for cornering effects on the slope estimation, the measured angular speed given by the IMU ω_{m_z} is also used. The applied motor torque, the measured bicycle speed, and the estimated road angle $\hat{\beta}$ are provided to the PTO expressed either in the form of a CPTO or a SPTO, to estimate the pedaling torque $\hat{T}_p$.

Based on the estimated pedaling torque, the vehicle speed, and road grade, different kinds of electrical assistance strategies may be applied to assist the vehicle motion and reduce the cycling efforts [27]. Since this work aims to analyze the accuracy of the estimation and the resulting cycling efforts reduction, a simple fixed-gain control strategy has been selected to minimize system complexity. This approach provides a torque reference $T_m^* = G\hat{T}_p$ as the set point for the motor torque control, where G represents the fixed-gain value.

B. ELECTRIC BICYCLE PROTOTYPE

The experimental validation of the torque-sensorless control approaches proposed in this work has been performed employing the electric bicycle prototype of Fig. 7. This vehicle mounts 28" tires ($r \simeq 0.35$ m) and a drivetrain with a fixed and known gear ratio $\tau_d = 2.8$. The electrical aid is provided through the *HS3540* hub direct-drive ($\tau_m = 1$) PMSM with superficially mounted magnets produced by *Crystalyte* and installed in the back wheel. The motor electrical parameters are reported in Table 1. Furthermore, the *SilverFish XH259* Li-Ion battery pack, produced by *Maratron*, with a maximum output voltage of 25.9 V and a capacity of 12 A·h has been selected. Moreover, the prototype includes the necessary electronics to control the motor, execute the estimation algorithms, and supervise the system. To perform these tasks, the electronics contain a *STM32H7* microcontroller from *STMicroelectronics*. The motor phase current measurements are implemented through in-line shunt resistors and current sensor amplifiers. The rotor position measurement is performed by using the *LM10* incremental magnetic rotary encoder from *RLS*. The inertial measurements are collected through the six-axis IMU *LSM6DSL* from *STMicroelectronics* firmly mounted to the bicycle frame. Furthermore, the pedaling torque sensor *ERST* from *ERider* is employed to measure the pedaling torque and validate the accuracy of the PTOs. Also, the prototype allows for signal visualization during operation through a monitor mounted on the bicycle handlebar and connected to a *Raspberry Pi4* single-board computer that communicates with the control electronics. Data collecting and streaming is possible through the software *ES:Scope* from *ES:Saar*.

C. ROAD SLOPE OBSERVER TUNING

As stated in Section IV-B, the proposed road slope estimation algorithm is based on the simplifying assumption that the vehicle acceleration a and the gravity acceleration longitudinal component g_x have a smaller bandwidth than the one of the state observer. A typical approach to handling modeling errors in a KF consists of weighing the confidence level on each equation through the covariance matrices [28]. In this case, more confidence can be given to the measurements v and a_{m_x} to compensate for the modeling simplifications. This means that the measurement equation variances must be chosen smaller than the ones of the process $\sigma_w^2 \gg \sigma_v^2$. Moreover, acceleration variations typically occur

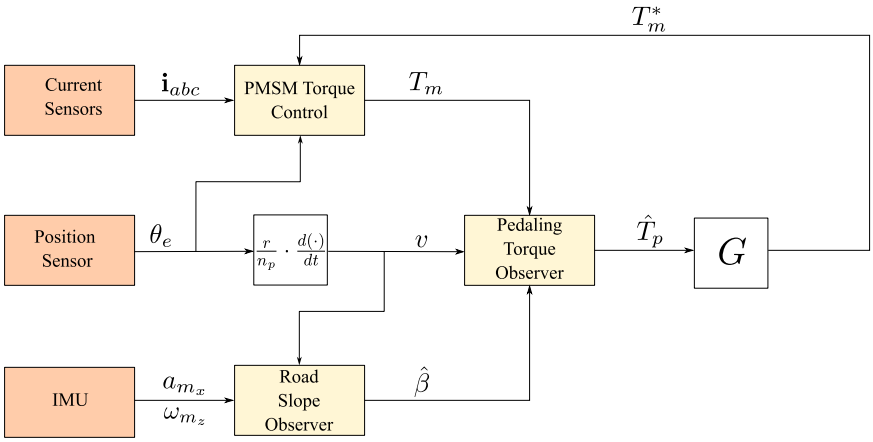

FIGURE 6. System description of the proposed torque-sensorless control for electric bicycles.

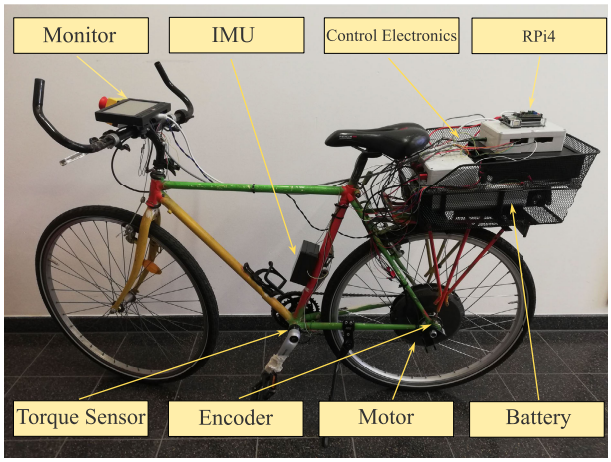

FIGURE 7. Designed electric bicycle prototype for the proposed torque-sensorless control validation.

TABLE 1. Motor electrical parameters of the *HS3540* hub direct-drive PMSM from *Crystalite Europe* mounted in the designed electric bicycle prototype.

Symbol	Motor parameter	Value
n_p	Number of pole pairs	23
R	Phase resistance	105 mΩ
L_d	Inductance d-axis	207 µH
L_q	Inductance q-axis	252 µH
Ψ_{PM}	Permanent magnet flux linkage	0.028 V · s
k_T	Torque constant	0.966 N · m/A
V_{DC_N}	Nominal DC voltage	48 V
I_{DC_N}	Nominal DC current	45 A
P_{m_N}	Nominal output power	2 kW
T_{m_N}	Nominal torque	80 N · m
ω_N	Nominal mechanical speed	25 rad/s

more rapidly than slope variations. Choosing $\sigma_{w_a}^2 \gg \sigma_{w_{gx}}^2$ allows to weigh the mistrust on each equation and reduce the effect of rapid acceleration changes on the estimated road slope. Based on the previous considerations, the following values for the covariance matrices have been selected in this work:

$$\mathbf{Q} = \begin{bmatrix} 100 & 0 & 0 \\ 0 & 1 & 0 \\ 0 & 0 & 1 \end{bmatrix} \quad \mathbf{R} = \begin{bmatrix} 0.01 & 0 \\ 0 & 0.01 \end{bmatrix}. \tag{30}$$

This estimation algorithm is digitally implemented on a microcontroller with a sampling frequency $f_s = 500$ Hz. Also, the algorithm measurements are low-pass filtered with a bandwidth of 1 Hz to reduce the effects of vibrations and differentiation on the slope estimation. Besides, the implemented curve compensation algorithm filters the estimated road slope with a bandwidth [0.005; 3] Hz depending on the measured aggressiveness of the curve. Table 2 contains the parameters utilized in the curve effect compensation approach. The reported values have been experimentally determined to reduce the estimation error when considering curves of different aggressiveness.

TABLE 2. Parameters utilized in the employed curve effect compensation method.

Tuning parameter	Value
Λ_{th}	0.1 rad/s
c	75
$f_{c_\beta}^{min}$	0.005 Hz
$f_{c_\beta}^{max}$	3 Hz

D. PEDALING TORQUE OBSERVER TUNING

The proposed PTOs contain modeling simplifications of the pedaling torque model. To account for this simplification, similarly to Section V-C, the confidence in the EKFs equations can be weighed by selecting the covariance matrices. In this case, more trust is given to the bicycle longitudinal dynamics model and the measured vehicle speed

to compensate for the pedaling torque model simplification $\sigma^2_{w_{T_p}}, \sigma^2_{w_{\dot{\xi}}} \gg \sigma^2_{w_v}, \sigma^2_{\nu_v}$. The covariance matrices of the PTOs have been chosen to minimize the Normalized Root Mean Square Error (NRMSE) of the estimated pedaling torque $\hat{T}_p$ concerning the average value of the measured pedaling $\bar{T}_p$. The normalization allows to compare the obtained results in different riding conditions where disparate pedaling torque levels are applied. Based on this criterium, the following values for the covariance matrices have been obtained experimentally:

$$\mathbf{Q} = \begin{bmatrix} 0.01 & 0 \\ 0 & 500 \end{bmatrix}, \quad R = 0.001, \tag{31}$$

in the case of the CPTO and

$$\mathbf{Q} = \begin{bmatrix} 0.01 & 0 & 0 & 0 \\ 0 & 500 & 0 & 0 \\ 0 & 0 & 500 & 0 \\ 0 & 0 & 0 & 500 \end{bmatrix}, \quad R = 0.001, \tag{32}$$

in the case of the SPTO.

Similarly to the road slope estimation, the PTOs are digitally implemented with a sampling frequency $f_s = 500$ Hz, and the measured vehicle speed is low-pass filtered with a bandwidth of 1 Hz. Moreover, the cyclist mass has been measured with a digital scale and its value has been updated in the microcontroller software before performing each experiment. Also, the pedaling torque estimation has been performed employing in the PTOs the rolling friction worst-case value $\mu = 0.01$ to account for bump losses, and the typical drag area of upright cycling $A_d = 0.63$ m^2 as defined in [27].

E. PERFORMED EXPERIMENTS DESCRIPTION

The proposed torque-sensorless control experimental validation is performed on a track, reported in Fig. 8, that covers approximately a distance of 200 m and is characterized by sections with variable slopes, curves, and level ground. Fig. 9 illustrates the estimated road slope obtained over the defined track employing the proposed KF. One can notice that the estimated road angle is contained approximately in the range $\beta \in [-0.5; 0.5]$ deg when riding on flat ground. Also, the track consists of rapid grade changes that sum up to the errors introduced by the cornering on the estimation. Thus, the selected track allows an analysis of the estimation algorithms and the electrical assistance within an exhaustive range of conditions that can be experienced in road cycling.

All the experiments have been executed riding the bicycle at an average target speed of circa $v \in [10; 15]$ km/h, displayed on the the prototype monitor. Furthermore, the tests have been performed in low wind speed conditions $|v_w| < 10$ km/h. The electrical assistance is provided by selecting a fixed gain $G = \frac{1}{\tau_d}$, namely, delivering a motor torque equal to the estimated or measured pedaling torque reported at the back wheel ($T_m = \frac{\hat{T}_p}{\tau_d}$ or $T_m = \frac{T_p}{\tau_d}$). For safety reasons during the testing phase, the motor current has been limited to $i_q = 20$ A, which means a maximum torque $T_m \simeq 20$ N·m

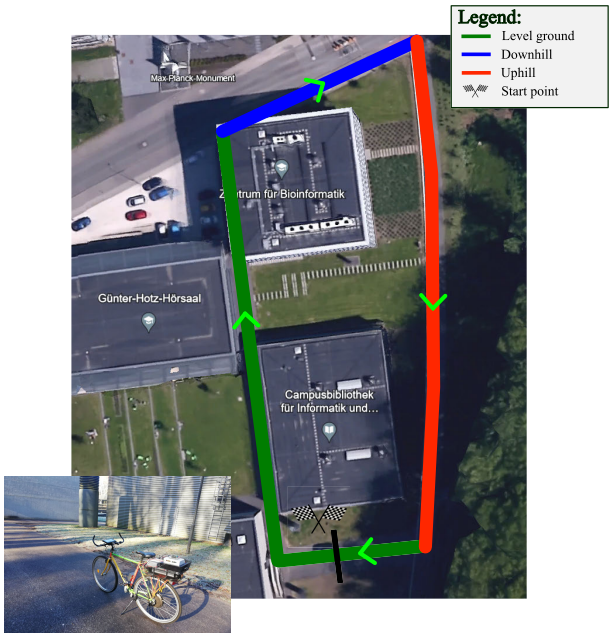

FIGURE 8. Selected track for the torque-sensorless control experimental validation (*Google* ©).

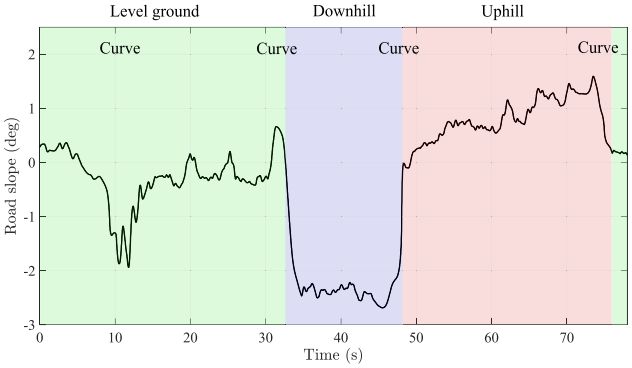

FIGURE 9. Estimated road slope on the track employed for the torque-sensoless control experimental validation.

can be delivered. Also, in the presence of estimated braking torques $\hat{T}_p < 0$ N·m, the electrical assistance is immediately cut off. It has to be remarked, that in each test, only one kind of assistance can be tested at a time since the cyclist adapts the delivered pedaling power to the received motor aid to achieve a desired target speed.

F. PEDALING TORQUE ESTIMATION

In this section, the NRMSE of the estimated pedaling torque is evaluated when riding in two noteworthy sections of the track where higher electrical assistance is typically required:

- **Starting phase**: riding on flat ground during the first 10 s of the experiment;
- **Uphill phase**: riding in the uphill section of the track.

Furthermore, the obtained pedaling torque estimation error is compared to the current state-of-the-art using the metric proposed in [14]. Three experiments have been performed in

TABLE 3. Confidence interval at 95% of the pedaling torque estimation NRMSE evaluated during the starting and uphill phases and reported at the back wheel.

NRMSE (%)		
PTO	**Starting phase**	**Uphill phase**
CPTO	72.55 ± 4.68	74.37 ± 0.49
SPTO	62.78 ± 7.58	66.87 ± 3.38

each condition, and the confidence intervals at 95% of the calculated NRMSE average values have been evaluated to account for the experiment variability and reported in Table 3. Fig. 10 contains examples of the pedaling torque estimated utilizing the CPTO and the SPTO in the before-mentioned riding conditions and reported at the back wheel (the torques are scaled of a factor $\frac{1}{\tau_d}$). In particular, the pedaling torque measured by the sensor T_p is compared to the estimated one $\hat{T}_p$. Also, in each condition, the estimated road grade $\hat{\beta}$ is reported in the figure.

As one can notice, the pedaling torque estimation NRMSE obtained with the SPTO results $5-10\%$ lower than the one achieved with the CPTO. Nevertheless, the SPTO estimates result more variable depending on the riding conditions. Furthermore, contrarily to the CPTO, the SPTO estimation keeps a pseudo-sinusoidal shape with a similar frequency to the measured signal, whereas the CPTO can only estimate approximately the pedaling torque average value.

The pedaling torque estimation analysis expressed in terms of NRMSE has shown that the proposed PTOs allow only an approximate estimation of the applied cycling torque with a performance improvement when a more detailed pedaling torque model is employed, namely when the SPTO is used. This result, which reflects the ones obtained in the current state-of-the-art of UIO-based pedaling torque estimators [14] and [19], can be explained by the simplifications made on the vehicle longitudinal dynamics and the pedaling torque models. Additionally, errors in the knowledge of model parameters and parametric variations while riding can be a further source of error. Moreover, the necessary low-pass filtering of the employed speed measurement to reduce the effect of vibrations and differentiation influences the road slope and pedaling torque estimation.

To compare the obtained results with the current state-of-the-art, the method employed in [14] that evaluates the Root Mean Square Error (RMSE) between the estimated pedaling torque at the crankset and the moving average of the measured torque using a sliding window of 0.7 s over the entire track is utilized. Considering three experiments performed under similar conditions, the confidence intervals at 95% of the RMSE have been calculated, resulting in 9.15 ± 0.6 N·m and 9.38 ± 0.69 N·m for the CPTO and SPTO, respectively. These results confirm that the CPTO can approximate slightly better than the SPTO the pedaling torque average value. Also, with both proposed PTOs, a performance estimation improvement of about 8% compared to the results obtained in [14] (RMSE $= 10.1$ N · m) has been achieved demonstrating the advantage of using the proposed approaches compared to the current state-of-the-art.

G. CYCLING POWER ANALYSIS

The accuracy of the pedaling torque estimation cannot be considered the only index to evaluate the cycling performance achieved with an electrical assistance method. The aim of the electrical assistance is indeed to reduce the cycling effort that can be related to the provided power reduction necessary to perform the riding task. Thus, this work analyzes the delivered cycling power P_p when the aid relies on the pedaling torque estimated with the CPTO and the SPTO. The achieved results are compared to the ones obtained without providing electrical assistance and with a sensor-based aid with fixed gain $G = \frac{1}{\tau_d}$. The peak $\max(P_p)$ and the average pedaling powers $\bar{P}_p$ are considered as metrics to evaluate the electrical assistance in the same portions of the track defined in Section V-F. These two quantities indicate the peak level and the overall intensity of the cycling effort on the considered track section, respectively. Additionally, to quantify the maximum and average pedaling power reduction of each assistance approach compared to the case without aid, two indexes have been defined, namely the Maximum Pedaling Power Reduction (MPPR) and the Average Pedaling Power Reduction (APPR):

$$\text{MPPR} = \left[1 - \frac{\max\left(P_{p_{\text{assistance}}}\right)}{\max\left(P_{p_{\text{no assistance}}}\right)}\right] \cdot 100, \tag{33}$$

$$\text{APPR} = \left(1 - \frac{\bar{P}_{p_{\text{assistance}}}}{\bar{P}_{p_{\text{no assistance}}}}\right) \cdot 100. \tag{34}$$

Also in this case, to account for experiment variability, the confidence interval at 95% of the average $\bar{P}_p$ and APPR over three experiments is evaluated. Whereas, in the case of the $\max(P_p)$ and the MPPR, the highest recorded peaks are analyzed since we are interested in evaluating the maximum cycling effort under defined conditions.

Fig. 11 illustrates examples of the delivered power during the starting phase of the track considering different kinds of assistance: no aid, sensor-based, CPTO-based, and SPTO-based assistance. Likewise, Fig. 12 depicts the delivered power in the uphill phase. Each sub-figure shows the measured pedaling power $P_p = \frac{T_p v}{\tau_d r}$, the delivered motor Power $P_m = \frac{T_m v}{r}$, the combined delivered power $P_T = P_p + P_m$, and the estimated road slope $\hat{\beta}$. Table 4 and Table 5 contain the pedaling power analysis in the starting and uphill sections of the track, respectively.

As one can see in Fig. 11(b) and Fig. 12(b), when providing electrical assistance relying on sensor measurements, the motor aid is an almost perfect amplification of the measured signal, except when the desired torque exceeds the maximum applicable torque limitation of the prototype. In this case, the total delivered power is about

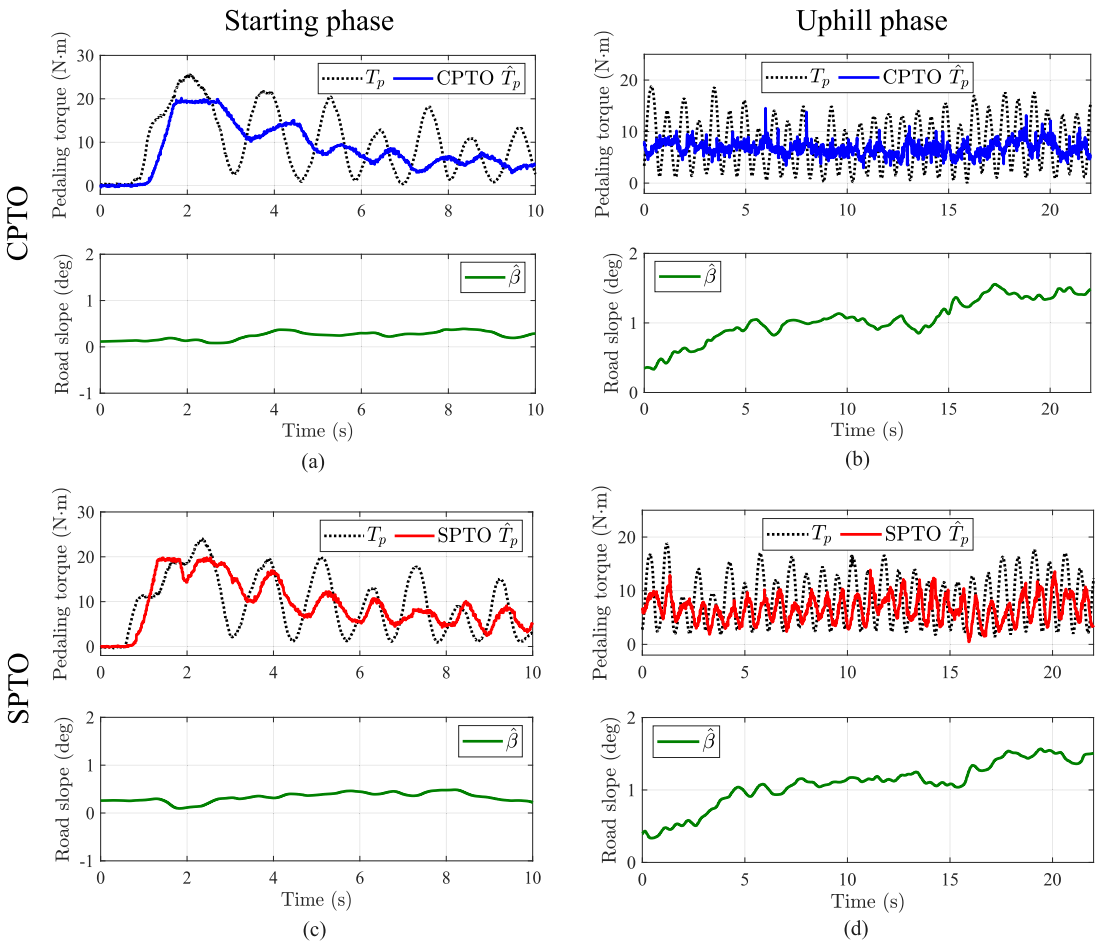

FIGURE 10. PTOs estimating pedaling torque reported at the back wheel when starting and riding uphill with electrical assistance. Figure (a) CPTO estimation when starting riding, Figure (b) CPTO estimation when riding uphill, Figure (c) SPTO estimation when starting riding, Figure (d) SPTO estimation when riding uphill.

TABLE 4. Pedaling power analysis in the starting phase of the track with different kinds of electrical assistance.

Type	max (P_p)(W)	$\bar{P}_p$ (W)	MPPR (%)	APPR (%)
No aid	246.34	84.3 ± 9.95	———	———
Sensor	160.61	54.06 ± 5.23	34.8	35.87 ± 0.3
CPTO	173.19	51.29 ± 4.86	29.69	39.15 ± 0.15
SPTO	161.01	50.9 ± 6.01	34.63	39.61 ± 0.17

TABLE 5. Pedaling power analysis in the uphill section of the track with different kinds of electrical assistance.

Type	max (P_p) (W)	$\bar{P}_p$ (W)	MPPR (%)	APPR (%)
No aid	322.67	147.7 ± 2.97	———	———
Sensor	195.2	88.78 ± 9.32	39.51	39.87 ± 0.1
CPTO	226.44	91.98 ± 5.03	29.82	37.7 ± 0.06
SPTO	228.21	90.9 ± 11.92	29.27	38.46 ± 0.13

$P_T \simeq 2P_p$. When torque-sensorless assistance is provided, due to the torque estimation inaccuracy, the motor assistance adds a pseudo-sinusoidal offset onto the pedaling power. The additional power contribution has a more constant profile in

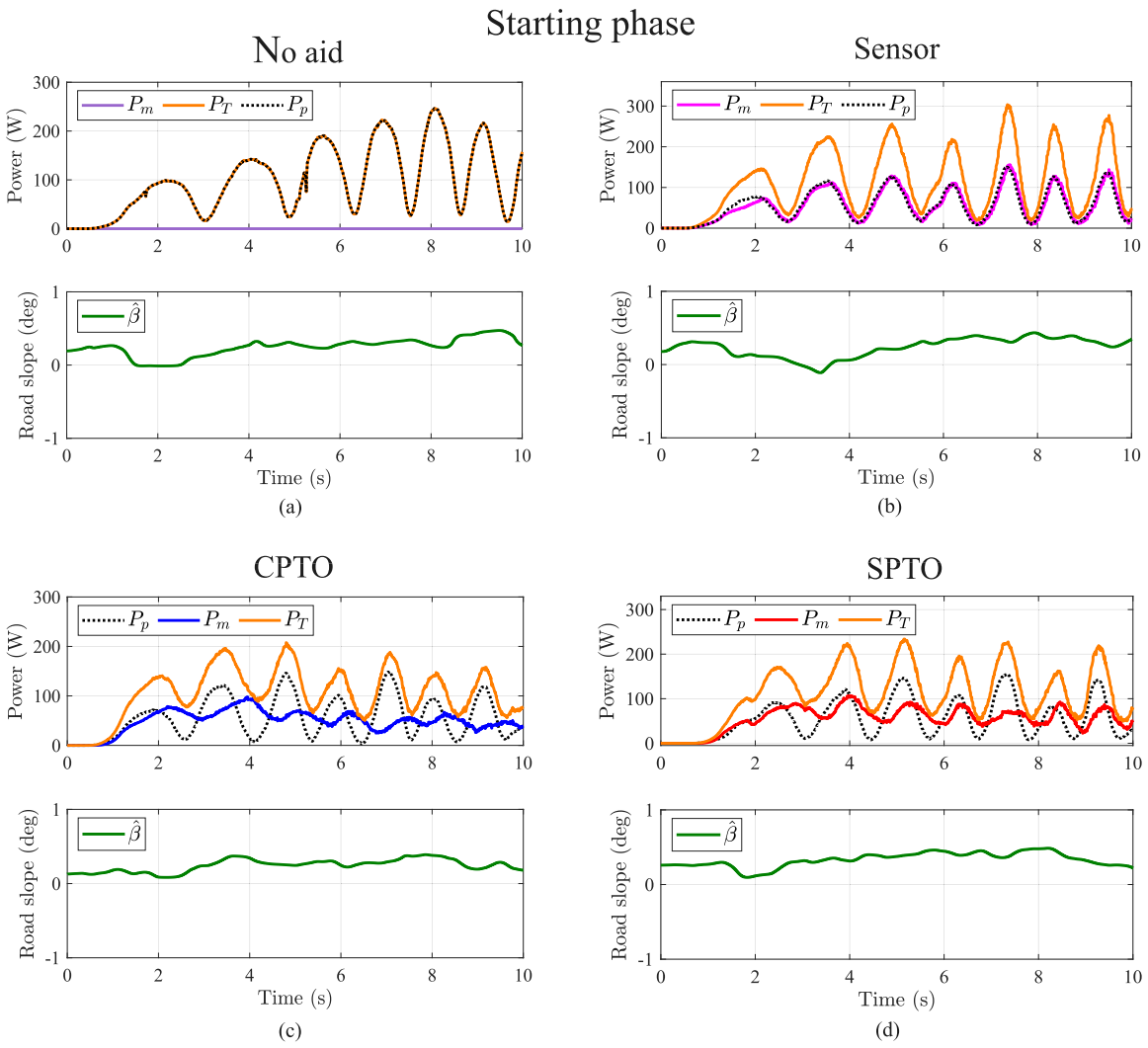

FIGURE 11. Delivered power in the starting phase of the track with different kinds of electrical assistance. Figure (a) no electrical assistance, Figure (b) sensor-based electrical assistance, Figure (c) CPTO-based electrical assistance, Figure (d) SPTO-based electrical assistance.

TABLE 6. Delivered energy analysis on the entire track with different kinds of electrical assistance.

Type	E_p (kJ)	E_m (kJ)	E_T (kJ)	PER (%)
No aid	22.61 ± 1.81	———	22.61 ± 1.81	———
Sensor	11.53 ± 1.58	11.44 ± 1.62	22.97 ± 3.2	49.8 ± 0.16
CPTO	12.78 ± 0.4	10.38 ± 0.32	23.15 ± 0.09	44.83 ± 1.51
SPTO	12.32 ± 1.9	10.89 ± 0.14	23.21 ± 1.84	47.1 ± 4.09

the case of CPTO-based assistance (Fig. 11(c) and Fig. 12(c)). Whereas, in the case of the SPTO-based one, the power offset is more reactive to the pedaling signal variations (Fig. 11(d) and Fig. 12(d)). Nonetheless, the total delivered power does not perfectly coincide with the one of the sensor-based assistance.

In Table 4, one can see that in the starting section, a similar APPR has been achieved for the two PTOs. With both torque-sensorless approaches, the average power reduction results even circa 5% higher than the one of the sensor-based assistance. This can be explained by the torque-filling effect caused by the inaccurate torque estimation of the PTOs. The electrical assistance is provided even at crank angles where typically low pedaling torque is applied. Moreover, one can notice that the MPPR results about 5% higher in the case of the SPTO-based assistance because the observer estimates

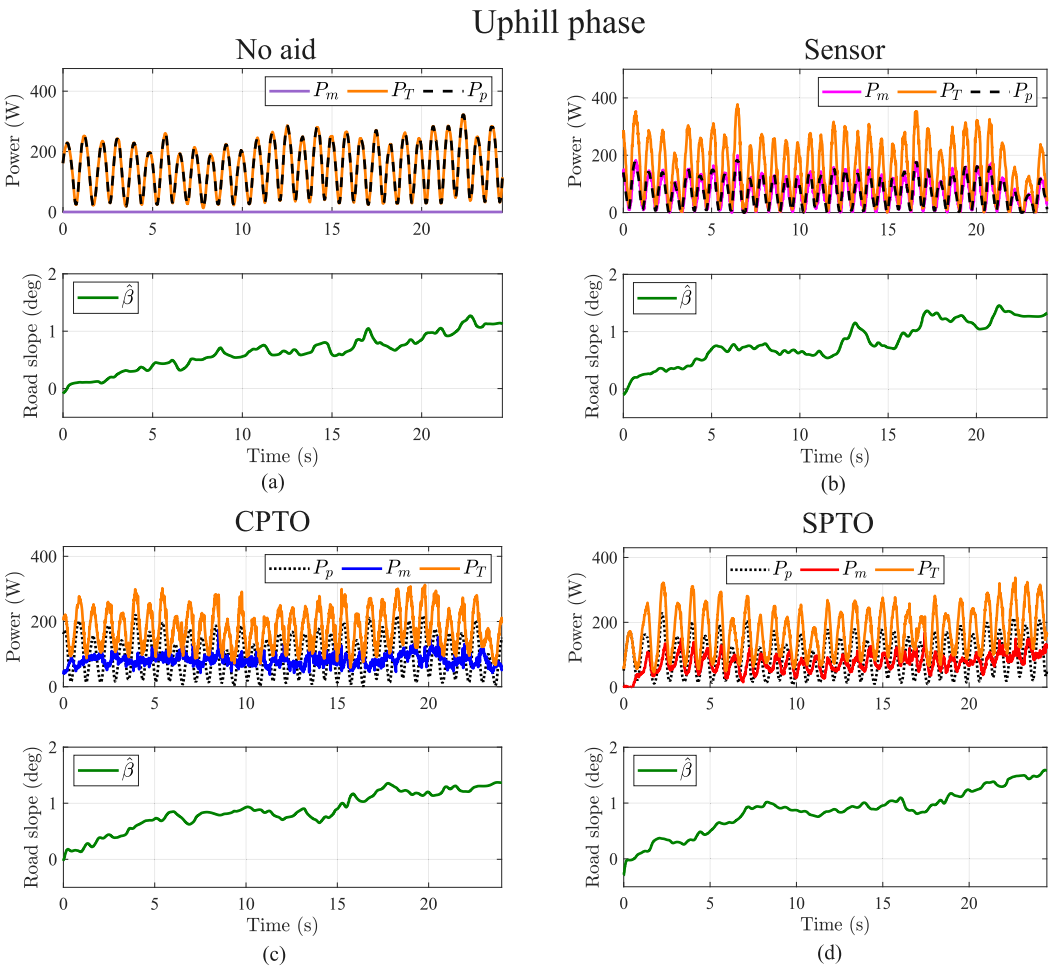

FIGURE 12. Delivered power in the uphill phase of the track with different kinds of electrical assistance. Figure (a) no electrical assistance, Figure (b) sensor-based electrical assistance, Figure (c) CPTO-based electrical assistance, Figure (d) SPTO-based electrical assistance.

the torque peaks with more accuracy than the CPTO. Also, its achieved MPPR is comparable to the one of the sensored aid.

From Table 5, one can see that in the uphill sector, the MPPR and APPR obtained with the sensor-based approach result circa 5% higher than the ones obtained in the starting phase because no saturation caused by the limitation of the motor torque has been experienced in the uphill portion of the track. Furthermore, it can be seen that the APPR worsens by circa $1-2\%$ for both torque-sensorless assistance methods compared to the starting phase. This degradation can be mainly explained by the effect of road slope estimation delays in a variable sloped environment and the required strong speed measurement filtering that reduces the average estimated pedaling torque even in the presence of the torque filling effect. The previously-mentioned delays also affect the torque peak estimation capability of both PTOs determining a MPPR reduction of circa 10% compared to the result obtained utilizing the sensor. In particular, a MPPR degradation of circa 5% has been achieved using the SPTO-based approach compared to the starting phase. Whereas, in the case of the CPTO-based aid, the estimation resulted less dependent on the aforementioned delays because comparable values have been achieved in both the starting and uphill portions of the track.

Despite the consistent pedaling torque estimation error, from the delivered power analysis, it can be concluded that small differences can be noticed between sensored and sensorless approaches in the absence of rapid road angle variations, like in the starting phase. Grade changes combined with the strong speed measurement filtering affect the pedaling peaks estimation capability rather than the average delivered power. Also, the SPTO-based electrical assistance results more similar to the sensored-based one during the starting phase. However, this resemblance degrades in the presence of rapid road slope variations. On the other hand, the CPTO-based assistance performances resulted less dependent on the angle estimation. Rapid angle variations and strong measurement filtering cannot be considered the sole source of error in the PTO estimates. As previously stated, parametric

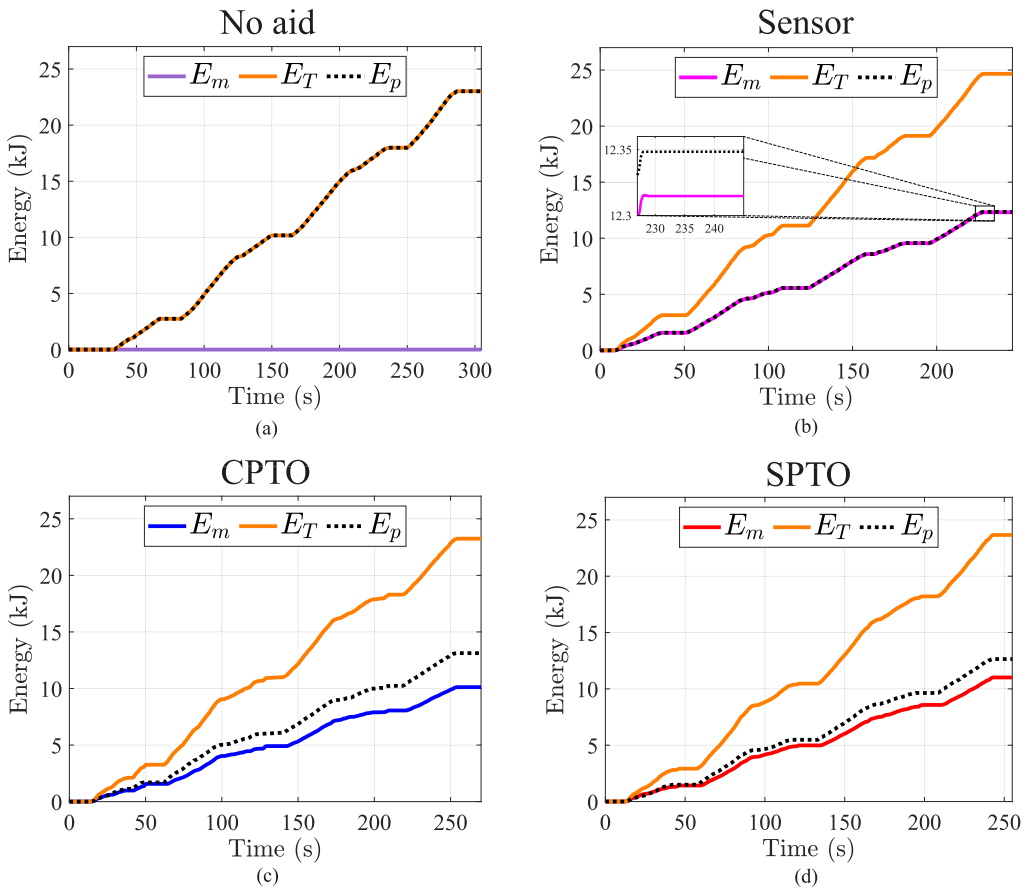

FIGURE 13. Delivered energy on three laps of the defined track with different kinds of electrical assistance. Figure (a) no electrical assistance, Figure (b) sensor-based electrical assistance, Figure (c) CPTO-based electrical assistance, Figure (d) SPTO-based electrical assistance.

variations and modeling simplifications may also be causes of performance degradation.

H. CYCLING ENERGY ANALYSIS

To evaluate the global pedaling effort required to perform the defined riding task, the total delivered energy with the different analyzed assistance approaches is investigated in this section. In particular, the pedaling energy E_p, the motor energy E_m, and the combined delivered energy $E_T = E_p + E_m$ are evaluated. Moreover, to quantify the pedaling effort reduction achieved with each kind of assistance, the Pedaling Energy Reduction (PER) index has been defined:

$$\text{PER} = \left(1 - \frac{E_p}{E_T}\right) \cdot 100. \tag{35}$$

This value indicates the cycling energy reduction compared to the total delivered energy when electrical assistance is provided. Also, to account for experiments variability, the confidence interval at 95% of each quantity is evaluated considering three trial rides composed of three laps of the defined track. Fig. 13 contains examples of the dissipated energy when using the different analyzed assistance types. The results of this energetic analysis are reported in Table 6.

As one can notice, the total delivered energy varies in each experiment depending on the applied cycling torque, the followed path, and the external conditions. Nevertheless, the final value is always within $E_T \in [20; 25]$ kJ. From the performed experiments, it emerged that, in the case of sensor-based assistance, the energy reduction amounts to circa 50% with reduced variability. Indeed, the employment of a pedaling torque sensor makes the received assistance independent of environmental conditions. Moreover, the PER would have been equal to 50% without motor torque saturation. In the case of CPTO-based assistance, the energy reduction degrades by circa 5% compared to the sensored assistance. Also, this degradation presents a higher variability because the pedaling torque estimation accuracy depends on external conditions. Utilizing the SPTO-based aid, the PER presents a reduction of only 3% compared to the sensored assistance. Nevertheless, its variability with environmental conditions results higher than the one achieved with the CPTO.

From a delivered energy perspective, the proposed sensorless approaches slightly increase the pedaling effort compared to sensor-based electrical assistance. Nonetheless, the effort reduction capability may be variable depending on

the environmental riding conditions, especially when a SPTO is considered.

VI. CONCLUSION AND OUTLOOKS

In this work, UIOs have been employed to address the problem of torque-sensorless control for electric bicycles. It has been shown that relying on a simplified bicycle longitudinal mathematical model, the reconstruction of the pedaling torque from the total disturbance acting on the system is possible without considerable performance degradation compared to sensored approaches. The results achieved with two pedaling torque models of different complexity are here analyzed and compared, namely a constant (CPTO) and a sinusoidal (SPTO) modeling. Furthermore, the problem of online road slope estimation has been addressed by utilizing a low-computational effort KF based on inertial and vehicle speed measurements. Experiments have been performed on an outdoor test track characterized by variable road slopes and curves. From the executed test rides, it emerged that a more accurate pedaling torque estimation is achievable when using a SPTO. Indeed, the NRMSE of the estimated pedaling torque has resulted about $5 - 10\%$ lower than the one obtained with the CPTO in the same riding conditions. Moreover, differently from the CPTO, which estimates approximately the pedaling torque average value, the SPTO estimation has a pseudo-sinusoidal shape with a similar frequency to the applied cycling torque. Also, both proposed PTOs have improved the pedaling torque average value estimation capability compared to the current state-of-the-art of UIO-based torque estimators of circa 8%. To evaluate the cycling effort reduction achieved with the proposed electrical assistance methods, this work analyzes the pedaling power and energy reduction as possible metrics. In particular, the maximum (MPPR) and average (APPR) power reduction when starting and during uphill riding and the global pedaling energy reduction (PER) to perform the defined riding task are evaluated. Despite the modeling simplifications and estimation errors, the electrical assistance provided relying on the PTOs estimate has allowed to achieve a comparable pedaling power and energy reduction to a sensor-based assistance. For instance, the PER obtained with the torque-sensorless control has resulted only 5% and 3% worse than the sensor when utilizing a CPTO and a SPTO as torque estimators, respectively. Although generally performing more similarly to the sensored-assistance, the SPTO-based one has shown a higher dependency on variable riding conditions. The proposed torque-sensorless control approaches might become a promising alternative to the employment of pedaling torque sensors that could save costs in electric bicycle applications. Nevertheless, some improvements are still required. Above all, the dependency on external conditions such as rapid road grade changes, strong headwinds, and vibrations should be reduced. Further works on this topic will address the improvement of road angle estimation and the avoidance of strong speed measurement filtering. Also, the inclusion of the wind in the vehicle longitudinal dynamics and an online estimation of the system parameters, such as mass, rolling friction coefficient, drag area, and gear ratio worth further investigation. However, when considering possible system enhancements, it is fundamental to evaluate the overall increase in costs and complexity to avoid losing the advantage of switching to sensorless approaches.

NOMENCLATURE

LIST OF ABBREVIATIONS

APPR	Average Pedaling Power Reduction.
BDC	Bottom Dead Center.
CPTO	Constant Pedaling Torque Observer.
DOB	Disturbance OBserver.
EKF	Extended Kalman Filter.
FOC	Field Oriented Control.
IMU	Inertial Measurement Unit.
KF	Kalman Filter.
MEMS	Micro-ElectroMechanical System.
MPPR	Maximum Pedaling Power Reduction.
NRMSE	Normalized Root Mean Square Error.
PER	Pedaling Energy Reduction.
PMSM	Permanent Magnet Synchronous Machine.
PTO	Pedaling Torque Observer.
RFO	Reaction Force Observer.
RLS	Recursive Least Squares.
RMSE	Root Mean Square Error.
SPTO	Sinusoidal Pedaling Torque Observer.
TDC	Top Dead Center.
UIO	Unknown Input Observer.
UKF	Unscented Kalman Filter.

LIST OF SYMBOLS

a	Bicycle longitudinal acceleration.
a_m	Measured IMU acceleration.
a_{m_N}	Normal to the trajectory IMU acceleration.
$a_{m_{N_x}}$	Measured longitudinal normal to the trajectory IMU acceleration.
a_{m_T}	Tangential to the trajectory IMU acceleration.
$a_{m_{T_x}}$	Measured longitudinal tangential to the trajectory IMU acceleration.
a_{m_x}	Measured longitudinal IMU acceleration.
a_{m_y}	Measured lateral IMU acceleration.
a_{m_z}	Measured vertical IMU acceleration.
A_d	Drag area.
c	Curve agressiveness calculation coefficient.
E_m	Motor energy.
E_p	Pedaling energy.
E_T	Total delivered energy.
f_{c_β}	Road slope estimation low-pass filter cutoff frequency.
$f_{c_\beta}^{max}$	Road slope estimation low-pass filter maximum cutoff frequency.
$f_{c_\beta}^{min}$	Road slope estimation low-pass filter minimum cutoff frequency.
f_s	Sampling frequency.

F_a	Aerodynamic drag force.
F_b	Braking force.
F_g	Gravity force.
F_h	Human forces.
F_h^e	Human forces others than pedaling.
F_m	Motor force.
F_p	Pedaling force.
F_p^l	Left pedaling force.
$F_{p_R}^l$	Left pedaling force radial component.
$F_{p_T}^l$	Left pedaling force tangential component.
F_p^r	Right pedaling force.
$F_{p_R}^r$	Right pedaling force radial component.
$F_{p_T}^r$	Right pedaling force tangential component.
F_r	Rolling friction force.
g	Gravity acceleration on Earth.
g_x	Gravity acceleration longitudinal component.
$\hat{g}_x$	Estimated gravity acceleration longitudinal component.
g_z	Gravity acceleration vertical component.
G	Electrical assistance fixed gain.
$G_\beta\ (s)$	Road angle estimation low-pass filter.
$G_{\omega_{m_z}}\ (s)$	Measured vertical IMU angular speed low-pass filter.
$\mathbf{i}_{abc}$	Motor phase current vector.
i_q	Motor q-axis current.
$\mathbf{I}$	Identity matrix.
I_{DC_N}	Nominal DC current.
k	Discrete time variable.
k_T	Motor torque constant.
l_c	Length of crank arm.
L_d	Motor d-axis inductance.
L_q	Motor q-axis inductance.
m	System mass.
n_p	Motor number of pole pairs.
$\mathbf{P}$	KF estimation error covariance matrix.
P_m	Motor power.
P_{m_N}	Motor nominal output power.
P_p	Pedaling power.
$P_{p_{\text{assistance}}}$	Pedaling power with electrical assistance.
$P_{p_{\text{no assistance}}}$	Pedaling power without electrical assistance.
$\bar{P}_p$	Average pedaling power.
$\bar{P}_{p_{\text{assistance}}}$	Average pedaling power with electrical assistance.
$\bar{P}_{p_{\text{no assistance}}}$	Average pedaling power without electrical assistance.
P_T	Total delivered power.
$\mathbf{Q}$	KF noise on the process covariance matrix.
r	Wheel radius.
R	PMSM phase resistance.
$\mathbf{R}$	KF noise on the measurements covariance matrix.
t	Continuous time variable.
T_m	Motor torque.
T_m^*	Control target motor torque.
T_{m_N}	Motor nominal torque.
T_p	Pedaling torque.
$\hat{T}_p$	Estimated pedaling torque.
$\bar{T}_p$	Pedaling torque average value.
T_p^l	Left pedal pedaling torque.
T_p^r	Right pedal pedaling torque.
T_{p_0}	Pedaling torque continuous component.
T_{p_2}	Pedaling torque second harmonic component.
T_s	Sampling time.
$\mathbf{u}$	Input vector.
v	Bicycle longitudinal speed.
v_a	Relative air longitudinal speed.
v_w	Wind longitudinal speed.
V_{DC_N}	Nominal DC voltage.
$\mathbf{w}$	KF noise on the process vector.
w_{T_p}	CPTO noise on the pedaling torque state equation.
w_a	KF noise on the acceleration state equation.
w_{g_x}	KF noise on the longitudinal gravity component state equation.
w_v	KF noise on the speed state equation.
w_{ξ_0}	SPTO noise on the pedaling torque continuous component state equation.
$w_{\xi_2^c}$	SPTO noise on the pedaling torque second harmonic cosine state equation.
$w_{\xi_2^s}$	SPTO noise on the pedaling torque second harmonic sine state equation.
$\mathbf{x}$	State vector.
$\mathbf{y}$	Output vector.
α	Auxiliary variable including the effect of road slope and rolling fricition.
β	Road slope.
$\hat{\beta}$	Estimated road slope.
β_μ	Rolling friction apparent slope.
η_d	Drivetrain transmission efficiency.
η_m	Motor transmission efficiency.
θ_c	Crank angle.
θ_e	Motor electrical angle.
Λ	Curve agressiveness index.
Λ_{th}	Curve agressiveness index threshold.
μ	Rolling friction coefficient.
ν	KF noise on the measurements vector.
$\nu_{a_{m_x}}$	KF noise on the measured IMU longitudinal acceleration.
ν_v	KF noise on the measured speed.
ξ_0	SPTO augmented state representing the pedaling torque continuous component.
$\hat{\xi}_0$	Estimated ξ_0.
ξ_2^c	SPTO augmented state representing the pedaling torque second harmonic cosine component.
$\hat{\xi}_2^c$	Estimated ξ_2^c.
ξ_2^s	SPTO augmented state representing the pedaling torque second harmonic sine component.
ρ	Air density.
σ_w^2	Variance of noise on the process.

$\sigma^2_{w_a}$	Variance of noise w_a.
$\sigma^2_{w_{g_x}}$	Variance of noise w_{g_x}.
$\sigma^2_{w_v}$	Variance of noise w_v.
$\sigma^2_{w_{T_p}}$	Variance of noise w_{T_p}.
$\sigma^2_{w_\xi}$	Variance of SPTO augmented state noise.
$\sigma^2_{w_{\xi_0}}$	Variance of noise w_{ξ_0}.
$\sigma^2_{w_{\xi_2^c}}$	Variance of noise $w_{\xi_2^c}$.
$\sigma^2_{w_{\xi_2^s}}$	Variance of noise $w_{\xi_2^s}$.
σ^2_v	Variance of noise on the measurements.
$\sigma^2_{v_{a_{m_x}}}$	Variance of noise $v_{a_{m_x}}$.
$\sigma^2_{v_v}$	Variance of noise v_v.
τ_d	Drivetrain gear ratio.
τ_m	Motor transmission gear ratio.
Ψ_{PM}	Motor permanent magnet flux linkage.
ω	Wheel angular speed.
ω_c	Crankset angular speed.
ω_e	Motor electrical angular speed.
ω_N	Motor nominal mechanical angular speed.
ω_{m_z}	Measured vertical IMU angular speed.

REFERENCES

[1] C. Contó and N. Bianchi, "E-bike motor drive: A review of configurations and capabilities," *Energies*, vol. 16, no. 1, p. 160, Dec. 2022.
[2] Y. Ruan, C. C. Hang, Y. M. Wang, and R. F. Ma, "The role of government in an emerging disruptive innovation: The case of E-bike in China," in *Proc. IEEE Int. Conf. Manage. Innov. Technol. (ICMIT)*, Bali, Indonesia, Jun. 2012, pp. 447–451.
[3] J. E. Bourne, S. Sauchelli, R. Perry, A. Page, S. Leary, C. England, and A. R. Cooper, "Health benefits of electrically-assisted cycling: A systematic review," *Int. J. Behav. Nutrition Phys. Activity*, vol. 15, no. 1, p. 116, Dec. 2018.
[4] J. Meditch and G. Hostetter, "Observers for systems with unknown and inaccessible inputs," in *Proc. IEEE Conf. Decis. Control Including 12th Symp. Adapt. Processes*, San Diego, CA, USA, Dec. 1973, pp. 120–124.
[5] K. Ohishi, K. Ohnishi, and K. Miyachi, "Torque-speed regulation of DC motor based on load torque estimation method," in *Proc. IPEC*, Tokyo, Japan, 1983, pp. 1209–1218.
[6] T. Murakami, F. Yu, and K. Ohnishi, "Torque sensorless control in multidegree-of-freedom manipulator," *IEEE Trans. Ind. Electron.*, vol. 40, no. 2, pp. 259–265, Apr. 1993.
[7] E. Sariyildiz and K. Ohnishi, "A comparison study for force sensor and reaction force observer based robust force control systems," in *Proc. IEEE 23rd Int. Symp. Ind. Electron. (ISIE)*, Istanbul, Turkey, Jun. 2014, pp. 1156–1161.
[8] V. Sankaranarayanan and S. Ravichandran, "Torque sensorless control of a human-electric hybrid bicycle," in *Proc. Int. Conf. Ind. Instrum. Control (ICIC)*, Pune, India, May 2015, pp. 806–810.
[9] T. Li, Q. Yang, X. Tu, and B. Ren, "An improved torque sensorless speed control method for electric assisted bicycle with consideration of coordinate conversion," *IEEE/CAA J. Autom. Sinica*, vol. 7, no. 6, pp. 1575–1584, Nov. 2020.
[10] D. S. Cheon and K. H. Nam, "Pedaling torque sensor-less power assist control of an electric bike via model-based impedance control," *Int. J. Automot. Technol.*, vol. 18, no. 2, pp. 327–333, Apr. 2017.
[11] T. Li, Q. Yang, B. Ren, and X. Tu, "A torque sensor-less speed control method of electric assisted bicycle," in *Proc. 37th Chin. Control Conf. (CCC)*, Wuhan, China, Jul. 2018, pp. 3705–3709.
[12] P. Padmagirisan, R. Sowmya, and V. Sankaranarayanan, "Power-assist control of a human–electric hybrid bicycle with energy regeneration and cruise control," *Proc. Inst. Mech. Eng., I, J. Syst. Control Eng.*, vol. 233, no. 2, pp. 179–191, Feb. 2019.
[13] R. Mandriota, S. Fabbri, M. Nienhaus, and E. Grasso, "Sensorless pedalling torque estimation based on motor load torque observation for electrically assisted bicycles," *Actuators*, vol. 10, no. 5, p. 88, Apr. 2021.
[14] B. J. E. Misgeld, L. Bergmann, B. Szilasi, S. Leonhardt, and D. Greven, "Virtual torque sensor for electrical bicycles," *IFAC-PapersOnLine*, vol. 53, no. 2, pp. 8903–8908, 2020.
[15] C. Johnson, "Accomodation of external disturbances in linear regulator and servomechanism problems," *IEEE Trans. Autom. Control*, vol. AC-16, no. 6, pp. 635–644, Dec. 1971.
[16] T. Kurosawa, Y. Fujimoto, and T. Tokumaru, "Estimation of pedaling torque for electric power assisted bicycles," in *Proc. IECON–40th Annu. Conf. IEEE Ind. Electron. Soc.*, Dallas, TX, USA, Oct. 2014, pp. 2756–2761.
[17] N. Fukushima and Y. Fujimoto, "Estimation of pedaling torque for electric power-assisted bicycle on slope environment," in *Proc. IEEE Int. Conf. Adv. Intell. Mechatronics (AIM)*, Munich, Germany, Jul. 2017, pp. 1682–1687.
[18] N. Fukushima and Y. Fujimoto, "Experimental verification of torque sensorless control for electric power-assisted bicycles on sloped environment," in *Proc. IEEE 15th Int. Workshop Adv. Motion Control (AMC)*, Tokyo, Japan, Mar. 2018, pp. 66–71.
[19] K. Hatada, K. Hirata, and T. Sato, "Energy-efficient power assist control with periodic disturbance observer and its experimental verification using an electric bicycle," *SICE J. Control, Meas., Syst. Integr.*, vol. 10, no. 5, pp. 410–417, Sep. 2017.
[20] W. C. Morchin and H. Oman, *Electric Bicycles: A Guide to Design and Use. Electric Bicycle Manual*. Piscataway, NJ, USA: Wiley, Nov. 2005.
[21] K. Hatada and K. Hirata, "Power assisting control for electric bicycles using an adaptive filter," in *Proc. IEEE Int. Conf. Ind. Technol. (ICIT)*, Busan, South Korea, Feb. 2014, pp. 51–54.
[22] S. Capmal and H. Vandewalle, "Torque-velocity relationship during cycle ergometer sprints with and without toe clips," *Eur. J. Appl. Physiol.*, vol. 76, no. 4, pp. 375–379, Sep. 1997.
[23] A. Muetze and Y. Tan, "Electric bicycles—A performance evaluation," *IEEE Ind. Appl. Mag.*, vol. 13, no. 4, pp. 12–21, Jul. 2007.
[24] A. Radke and Z. Gao, "A survey of state and disturbance observers for practitioners," in *Proc. Amer. Control Conf.*, Minneapolis, MN, USA, 2006, p. 6.
[25] W. Wang and Z. Gao, "A comparison study of advanced state observer design techniques," in *Proc. Amer. Control Conf.*, vol. 6, Denver, CO, USA, Jun. 2003, pp. 4754–4759.
[26] F. Auger, M. Hilairet, J. M. Guerrero, E. Monmasson, T. Orlowska-Kowalska, and S. Katsura, "Industrial applications of the Kalman filter: A review," *IEEE Trans. Ind. Electron.*, vol. 60, no. 12, pp. 5458–5471, Dec. 2013.
[27] D. G. Wilson and T. Schmidt, *Bicycling Science*, 4th ed., Cambridge, MA, USA: MIT Press, May 2020.
[28] D. Simon, *Optimal State Estimation: Kalman, H Infintiy, and Nonlinear Approaches*. Hoboken, NJ, USA: Wiley, Jan. 2006.
[29] M. Corno, P. Spagnol, and S. M. Savaresi, "Road slope estimation in bicycles without torque measurements," *IFAC Proc. Volumes*, vol. 47, no. 3, pp. 6295–6300, 2014.
[30] J. Jauch, J. Masino, T. Staiger, and F. Gauterin, "Road grade estimation with vehicle-based inertial measurement unit and orientation filter," *IEEE Sensors J.*, vol. 18, no. 2, pp. 781–789, Jan. 2018.

RICCARDO MANDRIOTA was born in Monopoli, Italy. He received the B.S. and M.S. degrees in automation engineering from the Politecnico di Bari, Italy, in 2016 and 2019, respectively. He is currently pursuing the Ph.D. degree in systems engineering with the Universität des Saarlandes, Saarbrücken, Germany. His research interests include control methods for light electric vehicles, sensorless control of electrical machines, system identification, and embedded systems.

NIKLAS KÖNIG was born in Völklingen, Germany. He received the B.S. and M.S. degrees in mechatronics and the Ph.D. degree in systems engineering from the Universität des Saarlandes, Saarbrücken, Germany, in 2014, 2016, and 2024, respectively. He is currently with the Lehrstuhl für Antriebstechnik, Universität des Saarlandes. His research interests include sensorless control of electrical machines, linear actuation technology, system identification, and embedded systems.

EMANUELE GRASSO was born in Foggia, Italy. He received the M.S. degree in automation engineering from the Politecnico di Bari, Italy, in 2008, the Ph.D. degree in mechatronics from the Universität des Saarlandes, Germany, in 2014, and the Habilitation degree, in 2021, with his work on sensorless control of electrical machines. He was a Professor in robotics with the IU Internationale Hochschule while being currently a Guest Professor in electrical machines and drives with the Universität des Saarlandes and, at the same time, leading research and development groups in the semiconductor industry. His research interests include condition monitoring and sensorless control of different electromagnetic actuators, such as machines and linear drives, including active magnetic bearings.

MATTHIAS NIENHAUS was born in 1963. He received the degree in watchmaker and precision engineering from the Fachhochschule Furtwangen, the degree in electrical engineering from the Universität Erlangen-Nürnberg, and the Ph.D. degree from the Institute for Microtechnology Mainz (IMM), in 1998. His professional carrier led him via Bosch, Siemens, IMM (the Head of the Department), mymotors & actuators GmbH (the Shareholder and Managing Director), and Faulhaber (the Area Director) to his current position as a Full Professor with Universiät des Saarlandes and the Head of the Lehrstuhl für Antriebstechnik LAT. At the LAT Department, he teaches and conducts research in the field of small and micro electromagnetic drives, with a focus on embedded drive systems and sensorless control. He is active in several VDE technical working groups and program committees of scientific congresses like Actuator. In November 2016, he founded the Steinbeis Transfer Center Embedded Drive Systems as a side activity to his university commitment for industrial technology transfer within the scope of research and development services until today. In February 2017, he founded the WELLGO Systems GmbH (Managing Director, Shareholder) with industrial partners as part of the well-established WELLGO Group for motorized assistance systems also as a side activity to his university commitment.